

## Partial widths of the $\text{He}^- 2S$ two-electron ionization ladder resonances

M. Chrysos, G. Aspromallis, Y. Komninos, and C. A. Nicolaides

*Theoretical and Physical Chemistry Institute, National Hellenic Research Foundation,  
48 Vassileos Constantinou Avenue, 116 35 Athens, Greece*

(Received 26 March 1992)

We present results for the partial and total widths, with interchannel and intrachannel coupling included, of the  $1s(nl)^2 2S$  resonances of  $\text{He}^-$ ,  $n=3$  and 4. These are obtained by solving the corresponding state-specific complex eigenvalue Schrödinger equations and subsequently using simple formulas. A number of conclusions are drawn as to the wave-function characteristics and the distribution of the autoionization rates. The computations include the self-consistent interactions between the core and the valence electrons, localized valence correlations, and interactions among all the open channels with helium  $1sNl^{3,1}L$ ,  $l=0,1,2$  cores. These prototypical calculations can be carried out in larger systems as well, since the structure of the theory is such that it allows the quantitative treatments of multichannel dynamics in arbitrary polyelectronic atoms. For the total widths, comparison is made with a previous 19-state  $R$ -matrix calculation and with measurements.

PACS number(s): 32.70.Jz, 31.50.+w, 32.80.Dz

### I. INTRODUCTION

The inner-shell-excited series of  $2S$  of  $\text{He}^-$ , whose assignment is a linear combination of  $1s(nl)^2$  configurations, constitutes a two-electron ionization ladder, (TEIL), as deduced from first-principles computations of their energies and wave functions [1,2]. Comparison with the electron scattering resonance data of Buckman *et al.* [3,4] verified that what was seen experimentally indeed corresponds to a series of doubly excited states with strong localization properties of the two valence electrons at equal distances from the nucleus and at an angle tending to  $180^\circ$  as the two-electron threshold is approached [1,2,5]. Such an identification had previously [3] been based on the good fitting of the observed energies to a Rydberg-like formula [6].

The fact that theory has been able to interpret the  $\text{He}^-$  experimental resonance spectrum in terms of the special class of Wannier TEIL states is indeed satisfactory. However, what is most challenging is the problem of obtaining reliably the characteristics of their decay dynamics. Here, no experimental data exist. How is energy redistributed and with what probability? More specifically, how can we compute the partial widths of the multitude of open channels available for decay, accounting for electronic structure, for interelectronic interactions, and for interchannel coupling?

It has been the objective of the present work to provide quantitative answers to such questions and to compare them with those pertaining to the  $\text{H}^-$  TEIL states of  $1S$  symmetry [7,8]. The interesting difference between  $\text{H}^-$  and  $\text{He}^-$  is the additional complexity due to the core electrons present in the closed and open channels of the  $\text{He}^- 2S$  resonances. Our earlier application to the  $\text{H}^- 1S$  TEIL [7,8] showed how partial widths *with interchannel coupling* can be obtained in a simple way and led to a

quantitative interpretation of the bulk of the decay dynamics of the TEIL resonances. Similar calculations have recently also been accomplished for the  $\text{H}^- 1P^\circ$  TEIL states [9], revealing a number of interesting properties common to both symmetries. One of these is the dominance of the nearest open channel, something which was first shown for the  $1S$  states [7] and also confirmed recently by Sadehghpour, Greene, and Canagnero [10] for  $\text{H}^- 1P^\circ$  resonances via eigenchannel  $R$ -matrix theory.

The part of the  $\text{He}^-$  TEIL spectrum which was considered in this study is shown in Fig. 1. The theory and computational methods for obtaining the correlated wave functions and the partial and total widths are discussed in the next two sections while Sec. IV contains our results and conclusions.

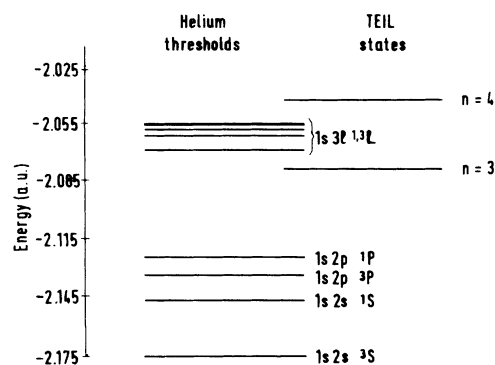


FIG. 1. Calculated positions of the  $n=3$  and  $\text{He}^- 2S$  TEIL states, in relation to the He thresholds into which they decay. The He  $1s^2$  ground state is outside the scale.

**II. BASIC FEATURES  
OF THE STATE-SPECIFIC THEORY  
FOR THE COMPUTATION  
OF CORRELATED WAVE FUNCTIONS  
OF RESONANCES IN POLYELECTRONIC ATOMS**

The reality of the electronic structure dependence of electron correlation in highly excited states, such as valence-excited autoionizing states or inner-hole Auger states, and the fact that these states decay into many open channels of the same symmetry, lead to one of the most demanding problems in the theory of atomic and molecular properties, i.e., the computation of partial widths of transitions to many interacting continua.

The theory and method of computation which are followed here solve this problem by diagonalizing suitably constructed non-Hermitian matrices with square-integrable function spaces and by subsequently using simple but rigorous formulas.

Specifically, for an isolated resonance we start with the complex eigenvalue Schrödinger equation (CESE)

$$(H - z_0)\Psi = 0, \quad (1a)$$

$$z_0 = E - \frac{i}{2}\Gamma, \quad (1b)$$

where  $\Psi$  satisfies unnormalizable asymptotic boundary conditions whose form depends on the potential ([11,12] and references therein). Projection of  $\Psi$  onto  $\Phi_0$ , the portion representing the interelectronic interactions contributing to the localization of the resonance [see Eqs. (1)–(30) of Ref. [13]], gives rise to a real eigenvalue many-electron problem under square-integrability boundary conditions,

$$(H_0 - E_0)\Psi_0 = 0, \quad (2)$$

where  $H_0$  is the projected effective Hamiltonian  $H_0 = QHQ$ ,  $Q = \Psi_0 \langle \Psi_0$ . Note that no projection onto exact target states is required—as it is in the Feshbach formalism and its implementation on two-electron resonances [14]. Rather, the effort is concentrated on obtaining localized zero-order and correlation functions which, by construction or core orbital orthogonalities, exclude open channels and lower states of the same symmetry.

The difference

$$X_{as} = \Psi - \Psi_0 \quad (3)$$

is the asymptotic correlation representing particle emission. The function space is a symmetry-adapted product of electronic-structure-dependent cores with channel-dependent “Gamow orbitals” [15,11,16], which are made square integrable via the transformation  $\rho = re^{i\theta}$  [12,17].

The form and computation of  $\Psi_0$  and of  $X_{as}$  depend crucially on the concept and reliable representation of a realistic zeroth-order vector which is optimized for the state of interest. Starting with the calculations of Ref. [13], where the analytic Hartree-Fock (HF) method of Roothaan was applied, it has been demonstrated in work from this institute [1,2,5,7,18,19] that for such highly excited states, HF or multiconfiguration Hartree-Fock (MCHF) solutions can indeed be obtained numerically or

analytically and that these represent optimal zeroth-order descriptions accounting for the major characteristics of the concerted electronic motion.

This approach secures the following.

(i) In contradistinction to diagonalization methods of Hermitian or non-Hermitian Hamiltonians with fixed basis sets, which have been applied extensively to two-electron systems, arbitrary electronic structures of systems with any number of electrons can be treated. Reviews of the state-specific methods which are applicable to excited states are given in Refs. [20,21].

(ii) Rather than searching for roots of diagonalized matrices satisfying various resonance conditions, the basic desideratum is convergence to a specific, electronic-structure-dependent square-integrable solution, expressing the *localization* of the resonance state. In this regard, the correspondence is made between the existence of the proper HF or MCHF zeroth-order solution satisfying the virial theorem, the physically imposed radial nodes (applicable to atoms and diatomics) and structure-dependent orthogonality constraints, and the existence of the localized wave function  $\Psi_0$ , embedded in the continuous spectrum.

(iii) Even in zeroth-order, the major features of the TEIL and other multiply excited states emerge clearly and quantitatively. (See Refs. [1,2,5,18] for doubly excited states and Refs. [22–24] for triply excited states.)

(iv) Given the orbital structure of the zeroth-order approximation to  $\Psi$ , many-electron analysis of  $\Psi_0$  and of  $X_{as}$  leads naturally to the concepts of localized and asymptotic correlation functions [15,11,16] which are associated with physically transparent contributions to the real energy of Eq. (1b) and to the partial widths making up  $\Gamma$  of Eq. (1b) [25].

**III. APPLICATION TO THE COMPUTATION  
OF THE PARTIAL WIDTHS  
OF THE He<sup>-</sup> 2S TEIL RESONANCES**

The localization and spectral properties of the He<sup>-</sup> 2S TEIL resonances have been demonstrated in previous work [1,2]. Their main features are revealed by their MCHF wave functions for each level of excitation,  $n$ , which have the structure

$$\Phi_{\text{MCHF}}^n = \sum_l \alpha_l u_{nl}, \quad l=0, 1, \dots, n-1, \quad (4)$$

where  $u_{nl} \equiv 1snl^2$ . The valence orbitals are computed while they are kept orthogonal to the HF orbitals of the triplet core states of He\*. The coefficients  $\alpha_l$  for  $n=3-9$  are shown in Table I. They are large and positive, contributing to constructive interference of many strongly mixed spherical harmonics which localizes the electrons on the Wannier ridge. A point to note is that as  $n$  increases, the major configuration ceases to be the  $1sns^2$  and is replaced by  $1snp^2$  at  $n=8$ .

Given the very good results obtained earlier for the H<sup>-</sup> 1S TEIL states [7] and the similarity of their structures to those of the He<sup>-</sup> 2S TEIL states [1], in this work we chose

TABLE I. Expansion coefficients of the  $\Phi_{\text{MCHF}}^n$  of the He<sup>-</sup> 2S resonances  $n = 3-9$ .

Configuration	$n = 3$	$n = 4$	$n = 5$	$n = 6$	$n = 7$	$n = 8$	$n = 9$
$1s(ns)^2$	0.849	0.793	0.739	0.696	0.655	0.612	0.579
$1s(np)^2$	0.525	0.591	0.631	0.646	0.657	0.653	0.649
$1s(nd)^2$	0.054	0.144	0.227	0.297	0.351	0.397	0.429
$1s(nf)^2$		0.031	0.064	0.100	0.129	0.192	0.226
$1s(ng)^2$			0.004	0.008	0.010	0.065	0.089
$1s(nh)^2$				0.001	0.001	0.021	0.032
$1s(ni)^2$					0.001	0.003	0.007
$1s(nk)^2$						0.001	0.002
$1s(nl)^2$							0.001

$$\Psi_0^n \approx \Phi_{\text{MCHF}}^n, \quad (5a) \quad \rho^\lambda e^{-\alpha\rho}, \quad \rho = re^{i\theta}, \quad \theta < 0, \quad (7)$$

$$E_0^n \approx E_{\text{MCHF}}^n. \quad (5b)$$

The asymptotic correlation function is written as

$$X_{\text{as}}^n(e) = \sum_{N < n} X_{\text{as}}^N(E) \quad (6a)$$

$$= \sum_{N=1}^{n-1} \sum_{l=0}^{N-1} \sum_{S=0}^1 c_{N,l,S}^n V_{Nl}^{L,S} \otimes g^{N,l,S}(E), \quad (6b)$$

where  $V_{Nl}^{L,S} = [1sNl]^{2S+1}L$  and each open channel is uniquely specified by a triple  $(N, l, S)$  for a given resonance  $n$ . The Gamow orbitals  $g^{N,l,S}(E)$  have been constructed by using different orthogonal basis sets  $\{v_i l\}_n$  of properly chosen complexified Slater-type functions (see below), with ten and eight basis functions for the  $n = 3$  and 4 He<sup>-</sup> resonances, respectively (Tables II–IV). These have been kept orthogonal to the orbitals of the He triplet states lying below, while they were not made orthogonal to the valence orbitals. This nonorthogonality gives rise to non-negligible terms of the form  $\langle nl|v_i l\rangle I(nl, Nl)$  and  $\langle nl|v_i l\rangle R^k(1s, nl; 1s, Nl)$  in the matrix elements of the He<sup>-</sup> TEIL resonances, where  $I$  and  $R^k$  denote one-body and two-body integrals, respectively.

In order to decrease the error propagation during the sequential orthogonalizations of the  $v_i l$  to one another and to the core orbitals of the lower thresholds, we applied the Gramm-Schmidt method analytically. The symmetry-adapted three-electron channel functions were formed by coupling the Gamow orbitals  $g^{N,l,S}$ , with the corresponding neutral helium parental states  $1sNl^{2S+1}L$ .

By making several trials for various values of the non-linear parameters  $\alpha$  and  $\theta$  of the complexified radial parts of the Slater-type functions

well-defined regions of stability of the width versus  $\alpha, \theta$  and basis-set size were obtained. The optimum values  $\alpha_{\text{opt}}, \theta_{\text{opt}}$ , and the size of the function space for each  $n$ , are shown in Table II. Having thus optimized the function space, the all-order partial complex energies are given by

$$z^{N,l,S} = \delta^{N,l,S} - \frac{i}{2} \gamma^{N,l,S} \\ = \frac{c_{N,l,S}^n}{c_{\text{MCHF}}^n} \langle \Phi_{\text{MCHF}}^n | H | V_{Nl}^{L,S} \otimes g^{N,l,S} \rangle, \quad (8)$$

where  $c_{N,l,S}^n$  and  $c_{\text{MCHF}}^n$  are the mixing coefficients with interchannel coupling,  $\delta^{N,l,S}$  is the partial energy shift, and  $\gamma^{N,l,S}$  is the partial width. The total width of each TEIL state is then the sum of the partial widths

$$\Gamma^n = \sum_N \gamma^N = \sum_N \sum_l \sum_S \gamma^{N,l,S}. \quad (9)$$

We note that, because of its smallness, the partial width to the  $1s^2$  threshold was computed separately, by the golden rule formula and a numerical HF scattering function.

#### IV. RESULTS AND CONCLUSIONS

The results of our calculations permit the following observations, in conjunction with our previous results on H<sup>-</sup> [7].

(i) For each TEIL resonance, as we move from an open-channel manifold  $N$  to another, the manifold contri-

TABLE II. Number of configurations used to describe the function spaces  $\Phi_{\text{MCHF}}^n$  and  $X_{\text{as}}^n$ , number of rotated Slater-type orbital (STO) functions used per open channel, and optimum values of the non-linear parameters  $\alpha, \theta$  in each complexified Slater-type orbital,  $v_i l$ .

$n$	$\Phi_{\text{MCHF}}^n$	$X_{\text{as}}^n$	No. STO per orbital	$\alpha_{\text{opt}}$	$\theta_{\text{opt}}$
3	3	50	10	0.5	-30°
4	4	88	8	0.2	-30°

TABLE III. Closed- and open-channel configurations participating in each of the function spaces  $\Phi_{\text{MCHF}}^n$  and  $X_{\text{as}}^n$ , for  $n=3$  and 4. As regards the orbitals describing the free electron, they have been constructed by using for each of the states  $n=3$  and 4 a different orthogonal basis set  $\{v_i l\}_n$  of properly chosen complexified Slater-type functions, with ten and eight basis function, respectively.

$n$	$\Phi_{\text{MCHF}}^n$	$X_{\text{as}}^n$
3	$1s(3s)^2$	$(1s)^2 v_{i,s}$
	$1s(3p)^2$	$(1s2s)^1 S v_{i,s}$
	$1s(3d)^2$	$(1s2s)^3 S v_{i,s}$
		$(1s2p)^1 P^o v_{i,p}$
4		$(1s2p)^3 P^o v_{i,p}$
		$(1s)^2 v_{i,s}$
		$(1s2s)^1 S v_{i,s}$
		$(1s2s)^3 S v_{i,s}$
	$1s(4s)^2$	$(1s2p)^1 P^o v_{i,p}$
	$1s(4p)^2$	$(1s2p)^3 P^o v_{i,p}$
	$1s(4d)^2$	$(1s3s)^1 S v_{i,s}$
	$1s(4f)^2$	$(1s3s)^3 S v_{i,s}$
		$(1s3p)^1 P^o v_{i,p}$
		$(1s3p)^3 P^o v_{i,p}$
$(1s3d)^1 D v_{i,d}$		
	$(1s3d)^3 D v_{i,d}$	

bution to the total width changes by an order of magnitude (Tables VI and VII). As  $N$  decreases, the contribution becomes less important. The largest contribution comes from the closest to the resonance open-channel

TABLE IV. Energies (in eV from the double ionization threshold) of the  $\text{He}^{-2}S$  and  $\text{H}^{-1}S$  TEIL states  $n=3$  and 4. For  $\text{He}^{-}$ , the energy of the  $1s \text{He}^+$  state has been subtracted.

$n=3$		$n=4$	
$\text{He}^{-}$	$\text{H}^{-}$	$\text{He}^{-}$	$\text{H}^{-}$
State-specific theory			
2.108 <sup>a</sup>	1.867 <sup>b</sup>	1.153 <sup>a</sup>	1.074 <sup>b</sup>
2.156 <sup>c</sup>	1.885 <sup>c</sup>	1.180 <sup>c</sup>	1.088 <sup>c</sup>
Other methods			
2.149 <sup>d</sup>	1.882 <sup>e</sup>	1.154 <sup>d</sup>	1.085 <sup>e</sup>
	1.882 <sup>f</sup>		1.079 <sup>g</sup>
	1.878 <sup>h</sup>		
	1.878 <sup>i</sup>		1.078 <sup>i</sup>
Experiment			
2.137 <sup>k</sup>		1.153 <sup>k</sup>	
2.138 <sup>j</sup>		1.143 <sup>j</sup>	

<sup>a</sup>Present work.

<sup>b</sup>Reference [7].

<sup>c</sup>Reference [1].

<sup>d</sup>Reference [32].

<sup>e</sup>Reference [26].

<sup>f</sup>Reference [27].

<sup>g</sup>Reference [28].

<sup>h</sup>Reference [29].

<sup>i</sup>Reference [30].

<sup>j</sup>Reference [31].

<sup>k</sup>Reference [4].

manifold,  $N=n-1$ , exceeding by far that of the others. This phenomenon was first noticed in the  $^1S$  and  $^1P^o$  TEIL resonances of  $\text{H}^{-}$  [7,9]. It is attributed to the rapidly increasing overlaps of the valence orbitals with the  $Nl$  orbitals of the He thresholds,  $1sNl$ , as  $N$  increases from  $N=1$  to  $N=n-1$ . The rapid increase comes from the  $N^2$  dependence of the average radius of the  $Nl$  orbital.

(ii) For the  $\text{He}^{-2}S$  TEIL states  $n \leq 7$ , the nearest group of open channels corresponds to the helium thresholds  $N=n-1$ . However, a drastic change occurs at  $n=8$ . The energy of this state,  $-2.01056$  a.u., is found to be slightly lower than most of the helium thresholds  $N=7$ . Thus, for  $\text{He}^{-2}S$  TEIL states  $n \geq 8$ , most of the He channels  $N=n-1$  are no longer open, and therefore they start contributing to the localized component of the total wave function. This phenomenon is expected to become more pronounced for higher  $n$ , since an increasing number of channels gradually close. The same situation has already been observed for the TEIL states of  $\text{H}^{-}$  [7,9]. It is still an open question whether and to what extent the new closed channels contribute additively to the width of the resonance, which is otherwise expected to decrease rapidly as soon as the most significant open channels close.

(iii) When compared with the total widths of the  $\text{H}^{-1}S$  TEIL states [7], the total widths of the  $\text{He}^{-2}S$  TEIL resonances are larger. This is mainly due to the doubling of the number of the open channels in the latter case. (The effective nuclear charge is practically the same in both

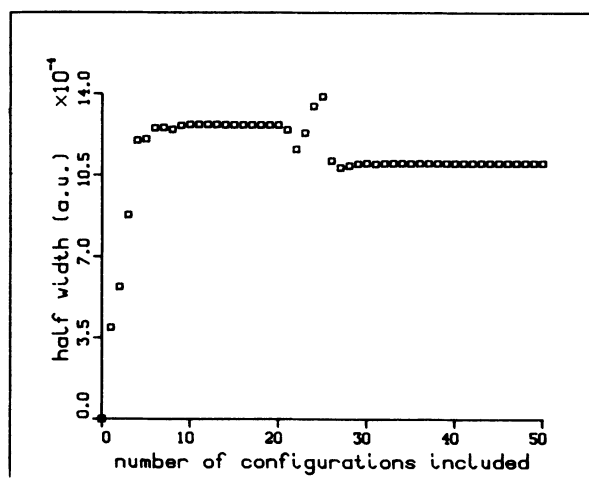


FIG. 2. Plot of the convergence of the autoionization half width (a.u.) of the  $n=3 \ ^2S$  TEIL state of  $\text{He}^{-}$ , as a function of the number of asymptotic correlation vectors used in the calculation. The first plateau represents a stable result reached as soon as all the  $p$ -type asymptotic functions have been included [20 functions:  $(1s2p)^1 P v_{i,p}$ ,  $(1s2p)^3 P v_{i,p}$ ,  $i=1, \dots, 10$ ]. The second plateau gives the half width of the resonance, and is reached as soon as all the  $s$ -type asymptotic vectors have also been added [30 functions:  $(1s2s)^1 S v_{i,s}$ ,  $(1s2s)^3 S v_{i,s}$ ,  $(1s)^2 v_{i,s}$ ,  $i=1, \dots, 10$ ]. The presence of the  $(1s)^2 \ e s$  channel does not affect at all the results which are obtained by the inclusion of all the  $N=2$  asymptotic channels.

TABLE V. Total autoionization widths (in meV) of the  $\text{He}^- 2S$  and  $\text{H}^- 1S$  TEIL states  $n=3$  and 4. The results correspond to the lowest root of each manifold. Our results show a slight decrease of the total width from  $n=3$  to 4 for both the  $\text{H}^- 1S$  and  $\text{He}^- 2S$  TEIL states. On the contrary, the  $R$ -matrix results of Ref. [32] show a fivefold increase, while the experimental values (Ref. [31]) for the two states are almost equal. Our result for the width of the  $\text{He}^- n=4$  TEIL state is in agreement with the experimental value, while that of the  $n=3$  state shows a discrepancy of 40%.

	$n=3$		$n=4$	
	State-specific complex eigenvalue theory			
This work	$\text{He}^-$	60	$\text{He}^-$	50
Ref. [7]	$\text{H}^-$	41	$\text{H}^-$	26
	Other methods			
	$\text{H}^-$		$\text{H}^-$	
Ref. [30]		41		30
Ref. [29]		39		
Ref. [28]				26
Ref. [32]	$\text{He}^-$	26	$\text{He}^-$	154
	Experiment			
Ref. [31]	$\text{He}^-$	36	$\text{He}^-$	50

systems, while the energy spectra tend to the same values as  $n$  increases [1].)

(iv) Despite the opening of more channels, in comparison with  $\text{H}^-$ , the tendency of the width to decrease as the level of excitation increases is similar to that of  $\text{H}^-$  (Table V). This is attributed to the gradually decreasing overlaps of the  $1s(nl)^2$  localized configurations with the various ‘‘asymptotic’’ configurations,  $1s(n-1)lv_i l$ . Indeed, the valence electrons are localized mainly in regions approximately proportional to  $n^2$ , while the Rydberg electrons of the remaining atom, for the closest to the resonance manifold, are mainly localized in radii approximately proportional to  $(n-1)^2$  and, therefore, the overlapping areas tend to decrease with increasing  $n$ .

(v) The various thresholds associated with each open-channel manifold are not degenerate any longer, as they were for  $\text{H}^-$  (Fig. 1). Now, their contribution to the width also depends on their distance from the corresponding TEIL state.

TABLE VI. Percentage of the total width of the  $(1sNl)^{1,3}L \epsilon l$  partial autoionization widths of the TEIL states  $n=3$  and 4 of  $\text{He}^- 2S$ . The contribution of each channel manifold,  $N$ , to the total width increases with increasing  $N$ , for any level of excitation,  $n$ . The  $p$  waves contribute the most.

Channels	$n=3$	$n=4$
$(1s)^2 \epsilon s$	1.6%	0.3%
$(1s2s)^3 S \epsilon s$	5.8%	0.1%
$(1s2s)^1 S \epsilon s$	2.7%	1.1%
$(1s2p)^3 P^\circ \epsilon p$	57.7%	1.7%
$(1s2p)^1 P^\circ \epsilon p$	32.3%	3.9%
$(1s3s)^3 S \epsilon s$		4.1%
$(1s3s)^1 S \epsilon s$		4.1%
$(1s3p)^3 P^\circ \epsilon p$		57.3%
$(1s3p)^1 P^\circ \epsilon p$		27.4%
$(1s3d)^3 D \epsilon d$		too small
$(1s3d)^1 D \epsilon d$		too small

(vi) Concerning the different parental terms within the mostly significant open-channel manifold,  $N=n-1$ , the triplets contribute to the total width almost twice as much as the singlets do (Table VI). This is due to the symmetry structure of the autoionization interaction matrix element.

(vii) From all the possible angular momentum channels within the channel manifold,  $N=n-1$ , the largest contribution comes from the  $p$  waves, while that of the  $d$  waves is negligible (Table VI).

(viii) As the number of open-channel configurations,  $(1sNl)^{2S+1}L v_i l$ , increases, the following result is observed. Each time the function space  $(1sNl)^{2S+1} \{v_i l\}_n$  is saturated for every specific  $n$ ,  $N$ , and  $l$ , a stable plateau is formed, which is associated with the partial width of the corresponding channel (Fig. 2). For example, consider the TEIL state at  $n=3$ . Having computed the localized  $\Psi_0^n$ , we sequentially add sets of ten functions each (Table III) of  $(1s2p)^3 P v_i p$ ,  $(1s2p)^1 P v_i p$ ,  $(1s2s)^3 S v_i s$ ,  $(1s2s)^1 S v_i s$ ,  $(1s)^2 v_i s$  channel configurations,  $i=1, 2, \dots, 10$ , thus obtaining different plateaus (Fig. 2). For the formation of each plateau, only part of the interthreshold channel coupling is taken into account, in terms of the corresponding configurations. Therefore the plateaus shown in Fig. 2 offer a picture of the partial decay rates. When all the channel configurations are present, the distribution is stabilized at the total width of the state.

(ix) Finally, for the case of total widths, comparison is possible with the measurements of Brunt, King, and Read [31] and the large, 19-state  $R$ -matrix scattering cal-

TABLE VII. Partial widths to the  $(1s)^2$  channel (in a.u.) of the TEIL state  $n=3$  and 4 of  $\text{He}^- 2S$ , obtained from the golden rule formula and numerical Hartree-Fock scattering functions.

$n=3$	$n=4$
$3.58 \times 10^{-5}$	$4.60 \times 10^{-6}$

culations of Fon *et al.* [32]. The absolute numbers are shown in Table V. We note that there is a qualitative difference. Whereas the *R*-matrix calculations show an increase of the total width as we go from the  $n = 3$  to the

$n = 4$  TEIL state [the ratio being  $\Gamma(n=4)/\Gamma(n=3)=5.92$ ], the present CESE theory predicts a slight reduction [ $\Gamma(n=4)/\Gamma(n=3)=0.83$ ], in agreement with the trend found for the  $^1S$  TEIL states of  $H^-$ .

- 
- [1] Y. Komninos, M. Chrysos, and C. A. Nicolaides, *J. Phys. B* **20**, L791 (1987).
- [2] C. A. Nicolaides, M. Chrysos, and Y. Komninos, *J. Phys. B* **21**, L73 (1988); *Phys. Rev. A* **39**, 1523 (1989).
- [3] S. J. Buckman, P. Hammond, F. H. Read, and G. C. King, *J. Phys. B* **16**, 4039 (1983).
- [4] S. J. Buckman and D. S. Newman, *J. Phys. B* **20**, L711 (1987).
- [5] Y. Komninos and C. A. Nicolaides, *J. Phys. B* **19**, 1701 (1986).
- [6] F. H. Read, *J. Phys. B* **10**, 449 (1977).
- [7] M. Chrysos, Y. Komninos, Th. Mercouris, and C. A. Nicolaides, *Phys. Rev. A* **42**, 2634 (1990).
- [8] C. A. Nicolaides and Y. Komninos, *J. Phys. B* **23**, L571 (1990).
- [9] M. Chrysos, Y. Komninos, and C. A. Nicolaides, *J. Phys. B* **25**, 1977 (1992).
- [10] H. R. Sadeghpour, C. H. Greene, and M. Canagnero, *Phys. Rev. A* **45**, 1587 (1992).
- [11] C. A. Nicolaides, Y. Komninos, and Th. Mercouris, *Int. J. Quantum Chem. Symp.* **15**, 355 (1981).
- [12] C. A. Nicolaides and S. Themelis, *Phys. Rev. A* **45**, 349 (1992).
- [13] C. A. Nicolaides, *Phys. Rev. A* **6**, 2078 (1972).
- [14] T. F. O'Malley and S. Geltman, *Phys. Rev.* **137**, A1344 (1965); A. Temkin and J. F. Walker, *ibid.* **140**, A1520 (1965).
- [15] C. A. Nicolaides and D. R. Beck, *Phys. Lett.* **65A**, 11 (1978); *Int. J. Quantum Chem.* **14**, 457 (1978).
- [16] C. A. Nicolaides and Th. Mercouris, *Phys. Rev. A* **32**, 3247 (1985); **36**, 390 (1987).
- [17] A. M. Dykhne and A. V. Chaplik, *Zh. Eksp. Teor. Fiz.* **40**, 1427 (1961) [*Sov. Phys. JETP* **13**, 1002 (1961)].
- [18] Y. Komninos, N. Makri, and C. A. Nicolaides, *Z. Phys. D* **2**, 105 (1986).
- [19] Th. Mercouris and C. A. Nicolaides, *J. Phys. B* **24**, L557 (1991).
- [20] D. R. Beck and C. A. Nicolaides, in *Excited States in Quantum Chemistry*, edited by C. A. Nicolaides and D. R. Beck (Reidel, Dordrecht, 1978), pp. 105 and 329.
- [21] C. A. Nicolaides, in *Quantum Chemistry; Basic Aspects, Actual Trends*, edited by R. Carbo (Elsevier, New York, 1989), p. 343.
- [22] Y. Komninos, M. Chrysos, and C. A. Nicolaides, *Phys. Rev. A* **38**, 3182 (1988).
- [23] C. A. Nicolaides, M. Chrysos, and Y. Komninos, *Phys. Rev. A* **41**, 5244 (1990).
- [24] C. A. Nicolaides, *J. Phys. B* **25**, L91 (1992).
- [25] C. A. Nicolaides, in *Applied Many-Body Methods in Spectroscopy and Electronic Structure*, edited by D. Musherjee (Plenum, New York, 1992), p. 233.
- [26] J. M. Rost and J. S. Briggs, *J. Phys. B* **22**, 3587 (1989).
- [27] L. Lipsky, R. Anania, and R. M. Connelly, *At. Data Nucl. Data Tables* **20**, 127 (1977).
- [28] Y. K. Ho and J. Callaway, *Phys. Rev. A* **34**, 130 (1986).
- [29] J. Callaway, *Phys. Rev. A* **26**, 199 (1982).
- [30] A. Pathak, A. E. Kingston, and K. Berrington, *J. Phys. B* **21**, 2939 (1988).
- [31] J. N. M. Brunt, G. C. King, and F. H. Read, *J. Phys. B* **10**, 433 (1977).
- [32] W. C. Fon, K. A. Berrington, P. G. Burke, and A. E. Kingston, *J. Phys. B* **22**, 3939 (1989).